the estimated absorbed dose in the gallbladder was 20 times lower than the estimate from human subject data sets because we could not remove the gallbladder of the mouse. Therefore, to evaluate the effective dose of [^{18}F]FACT in target organs, a whole-body PET scan of human subjects may be preferable as compared with the extrapolation from mouse experiments.

Clinical applicability of [^{18}F]FACT

The present whole-body PET study was performed using healthy elderly subjects and not patients with AD. Previously, Koole et al. speculated that if brain uptake of ^{18}F amyloid ligand increased by a factor of three, this will only influence estimation of the effective dose within 1%; however, when the subject had taken medication that changed the function of the hepatic metabolism, the estimated effective dose will vary with a larger range [10].

In the present series of PET studies, brain PET scans using the 3D mode were performed between the first and the second emission scan. Therefore, the injected dose for 2D whole-body scans was set to lower level than usual, and the averaged injected activity of 160.8 MBq corresponded to a radiation dose of 2.99 mSv per single administration. With regard to the optimal injected activity that can ensure sufficient image quality for clinical use, the peak noise-equivalent counts ratio (NECR) is often used in its determination. It has also been reported that the peak NECR in 2D mode was not reached with an acceptable range of injected activity, whereas in 3D mode, there was a distinct maximum for the NECR for which the corresponding injected activity was based on patient height and weight [19]. For the scanner used in our study, the NECR peak in 3D mode was reached at 4.44 kBq/ml using an 8,000-ml phantom [13]. When the subject's height and weight were assumed to be 170 cm and 60 kg, respectively, this assumption corresponded to the optimal injected dose of about 260 MBq. In a real situation, there exists the effect of the activity outside the axial FOV, and the optimal injected dose would be much lower. Injected activity indicates radiation dose; for example, 200 MBq indicates a radiation dose of 3.72 mSv. ICRP 62 [20] recommended that the maximum radiation dose that causes a 'minor to intermediate' increase of risk levels while preserving social benefit levels that are 'intermediate to moderate' has an effective limit of 10 mSv/year [20,21]. Thus, the maximum injectable activity is 537.6 MBq [^{18}F]FACT/year, and this injection dose limit allows two or three PET scans to be performed. Furthermore, amyloid imaging is mainly undertaken in elderly patients aged >50 years, even though for early detection of AD, patients aged <50 years will also have an amyloid PET scan. According to the guidance on medical exposures in medical and biomedical research by the European Commission [22], dose restrictions for patients aged over >50 years are not as strict as for younger patients. Therefore, considerably more multiple PET scans may be possible.

Conclusions

The effective dose of the ^{18}F-labelled amyloid imaging agent, [^{18}F]FACT, was found to be acceptable for clinical study.

Competing interests

The authors declare that they have no competing interests.

Authors' contributions

MS carried out the data analysis and interpretation and drafted the manuscript. TM, HT, YK and KY performed the study design and contributed to the intellectual discussion. NO, SF and RI performed the animal experiments and synthesis of PET probes. KF, SW, KH, MM and HA provided the clinical data. All authors read and approved the final manuscript.

Acknowledgements

We would like to thank Dr. Muneyuki Sakata from the Positron Medical Center, Tokyo Metropolitan Institute of Gerontology, and Dr. Hiroshi Watabe from the Cyclotron Radioisotope Center, Tohoku University, for their helpful advice regarding data analysis. This study was supported in part by Grants-in-Aid of Young Scientists (B) (no. 24700445) from the Ministry of Education, Culture, Sports, Science and Technology (MEXT), Japanese Government.

Author details

[1]Division of Medical Physics, Tohoku University School of Medicine, 2-1 Seiryo-machi, Aoba-ku, Sendai 980-8575, Japan. [2]Division of Cyclotron Nuclear Medicine, Cyclotron Radioisotope Center, Tohoku University, Sendai 980-8578, Japan. [3]Department of Pharmacology, Tohoku University School of Medicine, Sendai 980-8575, Japan. [4]Department of Geriatrics and Gerontology, Division of Brain Sciences, Institute of Development, Aging and Cancer, Tohoku University, Sendai 980-8575, Japan. [5]Division of Radiopharmaceutical Chemistry, Cyclotron Radioisotope Center, Tohoku University, Sendai 980-8578, Japan. [6]Clinical Research, Innovation and Education Center, Tohoku University Hospital, Sendai 980-8574, Japan.

Received: 23 January 2013 Accepted: 8 April 2013
Published: 24 April 2013

References

1. Hardy J, Selkoe DJ: **The amyloid hypothesis of Alzheimer's disease: progress and problems on the road to therapeutics.** *Science* 2002, 297:353–356.
2. Furumoto S, Okamura N, Iwata R, Yanai K, Arai H, Kudo Y: **Recent advances in the development of amyloid imaging agents.** *Curr Top Med Chem* 2007, 7:1773–1789.
3. Kudo Y, Okamura N, Furumoto S, Tashiro M, Furukawa K, Maruyama M, Itoh M, Iwata R, Yanai K, Arai H: **2-(2-[2-Dimethylaminothiazol-5-yl]ethenyl)-6-(2-[fluoro]ethoxy)benzoxazole: a novel PET agent for in vivo detection of dense amyloid plaques in Alzheimer's disease patients.** *J Nucl Med* 2007, 48:553–561.
4. Sakata M, Wu J, Toyohara J, Oda K, Ishikawa M, Ishii K, Hashimoto K, Ishiwata K: **Biodistribution and radiation dosimetry of the alpha7 nicotinic acetylcholine receptor ligand [^{11}C]CHIBA-1001 in humans.** *Nucl Med Biol* 2011, 38:443–448.
5. Deloar HM, Fujiwara T, Shidahara M, Nakamura T, Watabe H, Narita Y, Itoh M, Miyake M, Watanuki S: **Estimation of absorbed dose for 2-[F-18]fluoro-2-deoxy-D-glucose using whole-body positron emission tomography and magnetic resonance imaging.** *Eur J Nucl Med Mol Imaging* 1998, 25:565–574.
6. Sakata M, Oda K, Toyohara J, Ishii K, Nariai T, Ishiwata K: **Direct comparison of radiation dosimetry of six PET tracers using human whole-body imaging and murine biodistribution studies.** *Ann Nucl Med* 2013, 27:285–296.
7. Scheinin NM, Tolvanen TK, Wilson IA, Arponen EM, Nagren KA, Rinne JO: **Biodistribution and radiation dosimetry of the amyloid imaging agent ^{11}C-PIB in humans.** *J Nucl Med* 2007, 48:128–133.

8. Lin KJ, Hsu WC, Hsiao IT, Wey SP, Jin LW, Skovronsky D, Wai YY, Chang HP, Lo CW, Yao CH, Yen TC, Kung MP: **Whole-body biodistribution and brain PET imaging with [^{18}F]AV-45, a novel amyloid imaging agent–a pilot study.** *Nucl Med Biol* 2010, **37**:497–508.
9. Wong DF, Rosenberg PB, Zhou Y, Kumar A, Raymont V, Ravert HT, Dannals RF, Nandi A, Brasic JR, Ye W, Hilton J, Lyketsos C, Kung HF, Joshi AD, Skovronsky DM, Pontecorvo MJ: **In vivo imaging of amyloid deposition in Alzheimer disease using the radioligand ^{18}F-AV-45 (florbetapir [corrected] F 18).** *J Nucl Med* 2010, **51**:913–920.
10. Koole M, Lewis DM, Buckley C, Nelissen N, Vandenbulcke M, Brooks DJ, Vandenberghe R, Van Laere K: **Whole-body biodistribution and radiation dosimetry of ^{18}F-GE067: a radioligand for in vivo brain amyloid imaging.** *J Nucl Med* 2009, **50**:818–822.
11. O'Keefe GJ, Saunder TH, Ng S, Ackerman U, Tochon-Danguy HJ, Chan JG, Gong S, Dyrks T, Lindemann S, Holl G, Dinkelborg L, Villemagne V, Rowe CC: **Radiation dosimetry of beta-amyloid tracers ^{11}C-PiB and ^{18}F-BAY94-9172.** *J Nucl Med* 2009, **50**:309–315.
12. Furumoto S, Okamura N, Furukawa K, Tashiro M, Ishikawa Y, Sugi K, Tomita N, Waragai M, Harada R, Tago T, Iwata R, Yanai K, Arai H, Kudo Y: **A ^{18}F-labeled BF-227 derivative as a potential radioligand for imaging dense amyloid plaques by positron emission tomography.** *Mol Img Biol.* in press.
13. Fujiwara T, Watanuki S, Yamamoto S, Miyake M, Seo S, Itoh M, Ishii K, Orihara H, Fukuda H, Satoh T, Kitamura K, Tanaka K, Takahashi S: **Performance evaluation of a large axial field-of-view PET scanner: SET-2400W.** *Ann Nucl Med* 1997, **11**:307–313.
14. Watanuki S, Tashiro M, Miyake M, Ishikawa Y, Itoh M, Yanai K, Sakemi Y, Fukuda H, Ishii K: **Long-term performance evaluation of positron emission tomography: analysis and proposal of a maintenance protocol for long-term utilization.** *Ann Nucl Med* 2010, **24**:461–468.
15. Loevinger R, Budinger T, Watson E: *MIRD Primer for Absorbed Dose Calculations. Revised edn.* New York: The Society of Nuclear Medicine; 1991.
16. Cristy M, Eckerman KF: *Specific Absorbed Fractions of Energy at Various Ages from Internal Photon ources.* Oak Ridge: ORNL/TM; 1987:8381.
17. Stabin MG, Sparks RB, Crowe E: **OLINDA/EXM: the second-generation personal computer software for internal dose assessment in nuclear medicine.** *J Nucl Med* 2005, **46**:1023–1027.
18. Kirschner AS, Ice RD, Beierwaltes WH: **Radiation dosimetry of ^{131}I-19-iodocholesterol: the pitfalls of using tissue concentration data -reply.** *J Nucl Med* 1975, **16**:248–249.
19. Lartizien C, Comtat C, Kinahan PE, Ferreira N, Bendriem B, Trebossen R: **Optimization of injected dose based on noise equivalent count rates for 2- and 3-dimensional whole-body PET.** *J Nucl Med* 2002, **43**:1268–1278.
20. ICRP: *Radiological Protection in Biomedical Research.* Oxford: Pergamon; 1992.
21. Kimura Y, Simeon FG, Hatazawa J, Mozley PD, Pike VW, Innis RB, Fujita M: **Biodistribution and radiation dosimetry of a positron emission tomographic ligand, ^{18}F-SP203, to image metabotropic glutamate subtype 5 receptors in humans.** *Eur J Nucl Med Mol Imaging* 2010, **37**:1943–1949.
22. Directorate-General Environment NSaCP: **Guidance on medical exposures in medical and biomedical research.** In *Radiation Protection.* Brussels: European Commission; 1998:1–14.

doi:10.1186/2191-219X-3-32
Cite this article as: Shidahara *et al.*: Evaluation of the biodistribution and radiation dosimetry of the ^{18}F-labelled amyloid imaging probe [^{18}F] FACT in humans. *EJNMMI Research* 2013 3:32.

Journals of Gerontology: BIOLOGICAL SCIENCES
Cite journal as: J Gerontol A Biol Sci Med Sci. 2013 December:68(12):1482–1492
doi:10.1093/gerona/glt041

Advance Access publication May 8, 2013

Royal Jelly Prevents the Progression of Sarcopenia in Aged Mice In Vivo and In Vitro

Kaijun Niu,[1,2] Hui Guo,[3] Yinting Guo,[4] Satoru Ebihara,[5] Masanori Asada,[6] Takashi Ohrui,[7] Katsutoshi Furukawa,[6] Masakazu Ichinose,[8] Kazuhiko Yanai,[9] Yukitsuka Kudo,[10] Hiroyuki Arai,[6] Tatsuma Okazaki,[8] and Ryoichi Nagatomi[2]

[1]Lab of Nutritional Epidemiology, Department of Nutrition and Food Science, School of Public Health, Tianjin Medical University, Tianjin, People's Republic of China.
[2]Division of Biomedical Engineering for Health & Welfare, Tohoku University Graduate School of Biomedical Engineering, Sendai, Japan.
[3]Tianjin University of Sport, Tianjin, China.
[4]Department of Behavioral Medicine, Tohoku University Graduate School of Medicine, Sendai, Japan.
[5]Department of Internal Medicine and Rehabilitation Science, Tohoku University Graduate School of Medicine, Sendai, Japan.
[6]Department of Geriatrics and Gerontology, Division of Brain Sciences, Institute of Development, Aging and Cancer, Tohoku University, Sendai, Japan.
[7]Division of Geriatric Pharmacotherapy, Institute of Development, Aging and Cancer, Tohoku University, Sendai, Japan.
[8]Department of Respiratory Medicine, Tohoku University Hospital, Sendai, Japan.
[9]Department of Pharmacology, Graduate School of Medicine, Tohoku University, Sendai, Japan.
[10]Clinical Research, Innovation and Education Center, Tohoku University Hospital, Sendai, Japan.

Address correspondence to Kaijun Niu, MD, Lab of Nutritional Epidemiology, Department of Nutrition and Food Science, School of Public Health, Tianjin Medical University, 22 Qixiangtai Road, Heping District, 300070 Tianjin, People's Republic of China. Email: nkj0809@gmail.com

Sarcopenia is characterized by the age-related loss of muscle mass and strength. One of the mechanisms of sarcopenia is the loss in the function and number of muscle satellite cells. Royal jelly (RJ) is a health food used worldwide. To obtain better digestion and absorption than RJ, protease-treated RJ (pRJ) has been developed. RJ and pRJ have been suggested to have potential pharmacological benefits such as prolonging the life span and reducing fatigue. Because these effects may improve sarcopenia and the functions of satellite cells, we examined the effects of RJ or pRJ treatment on the skeletal muscles in an animal model using aged mice. In vivo, RJ/pRJ treatment attenuated the decrease in the muscle weight and grip strength and increased the regenerating capacity of injured muscles and the serum insulin-like growth factor-1 levels compared with controls. In vitro, using isolated satellite cells from aged mice, pRJ treatment increased the cell proliferation rate, promoted cell differentiation, and activated Akt intracellular signaling pathway compared with controls. These findings suggest that RJ/pRJ treatment had a beneficial effect on age-related sarcopenia.

Key Words: Aged mice—Sarcopenia—Satellite cells—Royal jelly—Insulin-like growth factor-1—Akt signaling.

Received September 3, 2012; Accepted March 1, 2013

Decision Editor: Rafael de Cabo, PhD

THE population of people aged 60 and older is currently growing at the rate of 2.6% per year, which is more than twice the rate of growth of the total population in the world (1). In general, aging is accompanied by frailty, functional limitations, and disabilities that interfere with the activities of daily life. These factors reduce the quality of life of the elderly patients and eventually cause their loss of autonomy in daily life. Sarcopenia is the age-related loss of the muscle mass and strength, which causes frailty, functional limitations in daily living, disabilities, and, finally, a higher mortality rate in the elderly patients (2).

Satellite cells are resident myogenic progenitors in the skeletal muscles. They play a central role in the growth and regeneration of the skeletal muscles (3). In response to stimulation, satellite cells form myoblasts, fuse together, and generate new fibers (4). The age-related functional disability and decrease in the number of satellite cells contribute to the development of sarcopenia (5). Thus, maintaining the functions of satellite cells and their numbers may reduce sarcopenia and, furthermore, may improve the regenerating capacity of the skeletal muscles in the elderly patients. However, to isolate satellite cells, specific cell surface markers were not available until recently (6).

Among the factors that stimulate satellite cells, insulin-like growth factor-1 (IGF-1) plays a central role. IGF-1 stimulates satellite cell proliferation, their differentiation into myoblasts, and, finally, their differentiation into myotubes (4). IGF-1 is the most important mediator of muscle growth and repair (7). Furthermore, a recent study suggested the potential of IGF-1 to improve sarcopenia in the elderly patients (7).

Worker honeybees produce royal jelly (RJ) in their hypopharyngeal and mandibular glands (8). RJ has been used worldwide for many years as commercially available medical products and health foods and has been considered beneficial to health. These days, a modified RJ product, protease-treated RJ (pRJ), has been developed to improve digestion and absorption compared with regular RJ. Accumulating evidence suggests that RJ is rich in a wide variety of nutrients, including vitamins, minerals, and more than 20 amino acids (9). RJ also has numerous potential pharmacological capacities, such as prolonging the life span (in mice and nematodes) (10,11) and reducing fatigue (12), hypertension (13), and hypercholesterolemia, as well as antioxidant and anti-inflammatory effects (8,14–16).

Because these effects of RJ might have a potential to improve sarcopenia and the functions of satellite cells (17–21), we hypothesized that RJ might have a beneficial effect on the prevention of sarcopenia. Furthermore, we hypothesized that this effect might involve IGF-1. To the best of our knowledge, few studies have examined the effects of RJ on muscles in elderly patients or aged animals or the relationship between RJ and IGF-1. Thus, in this study, we examined the effects of the RJ/pRJ on muscle weight, muscle strength, satellite cell functions, the regenerating capacity of the skeletal muscles in vivo and in vitro, and the involvement of IGF-1 in an animal model using aged mice.

Methods

Culture Conditions of Satellite Cells and Cell Proliferation Assay

Sorted satellite cells from untreated, aged mice were cultured in growth medium containing high-glucose Dulbecco's modified Eagle's medium with 20% fetal bovine serum (MP Biomedicals, Morgan Irvine, CA), 2.5 ng/mL basic fibroblast growth factor (Invitrogen, Eugene, OR), 100 U/mL penicillin, and 100 μg/mL streptomycin (Sigma, St. Louis, MO). Satellite cells under eight passages were used in this study. Differentiation was induced as previously shown with some modifications in differentiation medium containing high-glucose Dulbecco's modified Eagle's medium, 5% horse serum (Sigma), penicillin, and streptomycin for several days (22). RJ and pRJ were dissolved in water, sterilized by a filter, and then added to the culture medium at the following concentrations: 100, 200, 500, or 1000 μg/mL. Some cells were serum starved for overnight and then stimulated with 10 nM insulin (Sigma), which is a potent activator of Akt, for 5 minutes. The cells were cultured for 24, 48, or 72 hours, and the number of cells was determined by water-soluble tetrazolium-8 (WST-8, DOJINDO, Tokyo, Japan) assay using a cell-counting kit (23,24).

Mice and Dietary Treatment

Male C57BL/6 mice were obtained from Clea Japan (Tokyo, Japan) and maintained under specific pathogen-free conditions with unrestricted access to food and water. Experiments were carried out in accordance with guidelines established by the Tohoku University Committee on Animal Research. At the age of 21 months, mice were divided into five groups according to the diets provided for each group and maintained for the next 3 months, with 10 mice in each group. The five groups of diets were normal diet (controls), diet mixed with 1% weight RJ (1% RJ), diet mixed with 5% weight RJ (5% RJ), diet mixed with 1% weight pRJ (1% pRJ), and diet mixed with 5% pRJ (5% pRJ). All diets were manufactured by Oriental Yeast Co., Ltd. (Chiba, Japan), stored at 4°C, and sealed in plastic bags in vacuo until use to avoid oxidation. The base diet was composed of 20% milk casein, 0.3% cystine, 39.7% starch, 13.2% a-starch, 10% sucrose, 0.0014% cellulose, 1% vitamins, 3.5% mineral mixture, 0.25% choline bitartrate, and 0.5% *tert*-butylhydroquinone. The amounts of milk casein and starch were adjusted to equalize total proteins and calories between the groups in accordance with the amounts of added RJ/pRJ. Therefore, total energy and protein levels per weight were the same in all the diet groups. However, the amino acid contents were different among the groups. Dried RJ and pRJ powder was supplied by Institute for Bee Products & Health Science (Okayama, Japan). The vitamin and mineral components of RJ and pRJ were analyzed by Japan Food Research Laboratories (Tokyo, Japan) and are shown in Table 1. The mice had unrestricted access to food and water. After 3 months of the diet treatment, the grip strength was measured. Then, 25 mice (five mice from each group) were anesthetized and sacrificed, their sera were collected, and skeletal muscle samples were isolated. The other 19 (≥ 3 mice from each group) mice were sacrificed for evaluation of the regenerating capacity of injured skeletal muscles at 5 days after the injury.

Wire Hang Test

A wire mesh grid (10 × 10 cm) was used to assess the muscle strength. The mouse was placed on the wire mesh, then the mesh was inverted, and the mouse was forced to hang on the wire using its four limbs. The longest hanging time was recorded as the duration. The previously mentioned measuring process was repeated until the mouse could not hang on the wire mesh after the inversion. The number of repeated times is shown as the number of times (25).

Muscle Injury Model

After 3 months of the diet treatment, mice were anesthetized, and cardiotoxin from *Naja mossambica mossambica* (Sigma) dissolved in 100 μL phosphate-buffered saline (PBS) (10 μM) was injected into the tibialis anterior (TA) muscle. Five days later, the mice were sacrificed; and the

Table 1. Vitamin and Mineral Composition of Royal Jelly Products (mg/100 g)

Components	Royal Jelly	Protease-Treated Royal Jelly
Minerals		
Sodium	40.2	2050
Phosphorus	662	580
Iron	3.21	2.8
Calcium	40.6	44.8
Potassium	814	766
Magnesium	90.9	74.3
Copper	1.34	0.91
Zinc	6.61	5.62
Manganese	0.22	0.17
Selenium	>0.005	0.006
Vitamins		
Thiamine	0.96	0.84
Riboflavin	2.03	1.92
Vitamin B6	1.12	0.63
α-Tocopherol	0.1	>0.1
Folic acid	0.12	0.06
Pantothenic acid	12.8	14.5
Biotin	0.0467	0.0722
Inositol	>2	41
Niacin	14.8	15.4
Choline	620	480

TA muscles were isolated, frozen in 2-methylbutane precooled in liquid nitrogen, and stored at −80°C for following histological analysis (26).

Measurements of Muscle Weight and Isolation of Satellite Cells

The satellite cells were isolated according to a previous study (6) with some modifications. The large hindlimb muscles of mice including the TA muscle, triceps surae muscle, quadriceps muscle, biceps femoris muscle, gluteus maximus muscle, and iliopsoas muscle were isolated, and the weights of the muscles were measured. Next, nonmuscle tissues were removed under a dissection microscope; the muscles were subjected to enzymatic dissociation with 0.2% collagenase Type II (Worthington Biochemical Corporation, Lakewood, NJ) for 60 minutes and then with 0.04 U/mL dispase (Gibco BRL, Grand Island, NY) for 45 minutes. The cell suspension was filtered through a cell strainer (BD Bioscience, Franklin Lakes, NJ), incubated with antimouse CD16/CD32 monoclonal antibody (mAb, 2.4G2, BD Bioscience) to block Fc receptors and then with the following antibodies: fluorescein isothiocyanate–labeled anti-CD31, anti-CD45 (BD Bioscience), anti-CD11b, and anti-Sca-1 antibodies (eBioscience, San Diego, CA); PE-labeled anti-integrin-α7 (MBL, Nagoya, Japan); and Alexa 647-labeled anti-CD34 (BD Bioscience). The cells were counted and sorted by FACSAria II flow cytometer (BD Bioscience) as previously shown (27).

Immunohistochemistry and Immunocytochemistry

Frozen muscle tissues were sectioned from a region approximately 3 mm from the top of the TA muscle (8 μm in thickness) using a cryostat. For embryonic myosin heavy chain (eMyHC) staining, frozen sections or cultured cells were fixed with acetone/methanol (50%/50%) for 30 seconds at −20°C. Specimens were blocked with 1% bovine serum albumin and 0.1% Triton X-100 in PBS at room temperature for 45 minutes and then incubated with anti-eMyHC antibody (F1.652, DSHB, Iowa City, IA) at 1:2 dilution at 4°C overnight, followed by Rodamine-conjugated secondary antibody staining (Chemicon International, Temecula, CA) at room temperature in the dark for 1 hour. For PAX7 staining, cultured cells were fixed with PBS containing 4% paraformaldehyde at room temperature for 20 minutes and then blocked with 1% bovine serum albumin and 0.1% Triton X-100 in PBS at room temperature for 45 minutes. After blocking, the cells were incubated with anti-Pax-7 antibody (R&D Systems, Minneapolis, NE) at 1:50 dilution at 4°C overnight followed by Alexa 488–coupled antimouse IgG antibody (Invitrogen) at 1:200 dilution at room temperature for 1 hour. Finally, the sections or cells were mounted in Vectashield Mounting Medium with 4′,6-diamidino-2-phenylindole (DAPI) (Vector labs, Burlingame, CA). In vivo, the regenerating capacity of the injured skeletal muscles was evaluated by quantifying the percentage of eMyHc-immunoreactive area per field (28). Ten randomly selected fields at ×200 magnification were measured in each sample. ImageJ software was used to quantify the eMyHC-immunoreactive areas per field. In vitro, the degree of differentiation of satellite cells of the aged mice was evaluated by the maximum diameter of the cells by Adobe Photoshop CS2 software (San Jose, CA). The muscle sections were stained for hematoxylin and eosin also. Images were taken using a phase-contrast and fluorescence microscope BZ9000 (Keyence, Osaka, Japan) (29).

Western Blot Analysis

PAX7, Type I IGF receptor (IGF-IR), Akt, and phosphorylated Akt (phospho-Akt) proteins were detected by Western blot analysis. In brief, the cells were rinsed twice with ice-cold PBS and lysed using RIPA Lysis Buffer (Upstate, Temecula, CA). The extracted protein fraction was electrophoresed in a sodium dodecyl sulfate and 10% polyacrylamide gel and then transferred onto an Immobilon transfer membrane (Millipore, Bedford, MA). The amount of protein loaded onto the gels was 36 μg per well. The membranes were immunoblotted with the primary antibodies to PAX7 (DSHB) at 1:100 dilution, GAPDH, IGF-IR, Akt, and phospho-Akt (Cell Signaling, Boston, MA) at 1:1000 dilution. Then, the membranes were incubated with horseradish peroxidase–conjugated antirabbit immunoglobulin G (Cell Signaling) at 1:25,000 dilution, and the protein bands were detected with an

enhanced chemiluminescence detection kit (Amersham, Buckinghamshire, UK) (30).

Enzyme-Linked Immunosorbent Assay

After RJ/pRJ treatment, the mice were anesthetized with diethyl ether, and blood samples were isolated from the inferior vena cava. The serum levels of interleukin-1α (IL-1α), IL-1β, IL-6, tumor necrosis factor-α, and IGF-1 were measured using a specific ELISA kit (R&D Systems) according to the manufacturer's instructions, respectively (22).

Statistical Analysis

Data are presented as mean ± standard deviation. Differences were analyzed by one-way analysis of variance test (Post hoc, Tukey). A level of $p < 0.05$ was accepted as statistically significant. All in vitro experiments were repeated at least three times.

Results

Isolation and Characterization of Satellite Cells

As an initial step, we tried to identify the effect of RJ/pRJ on satellite cells. The characterization of satellite cells by cell surface markers has been established only very recently (6). Therefore, according to that study, we first tried to isolate satellite cells with some modifications. We enzymatically dissociated mononuclear cells from the mouse hind-limb muscles (Figure 1A, circle: upper muscles were isolated from a right leg, and lower muscles were isolated from a left leg, from left to right, TA, triceps surae, quadriceps, divided biceps femoris into two, gluteus maximus, and

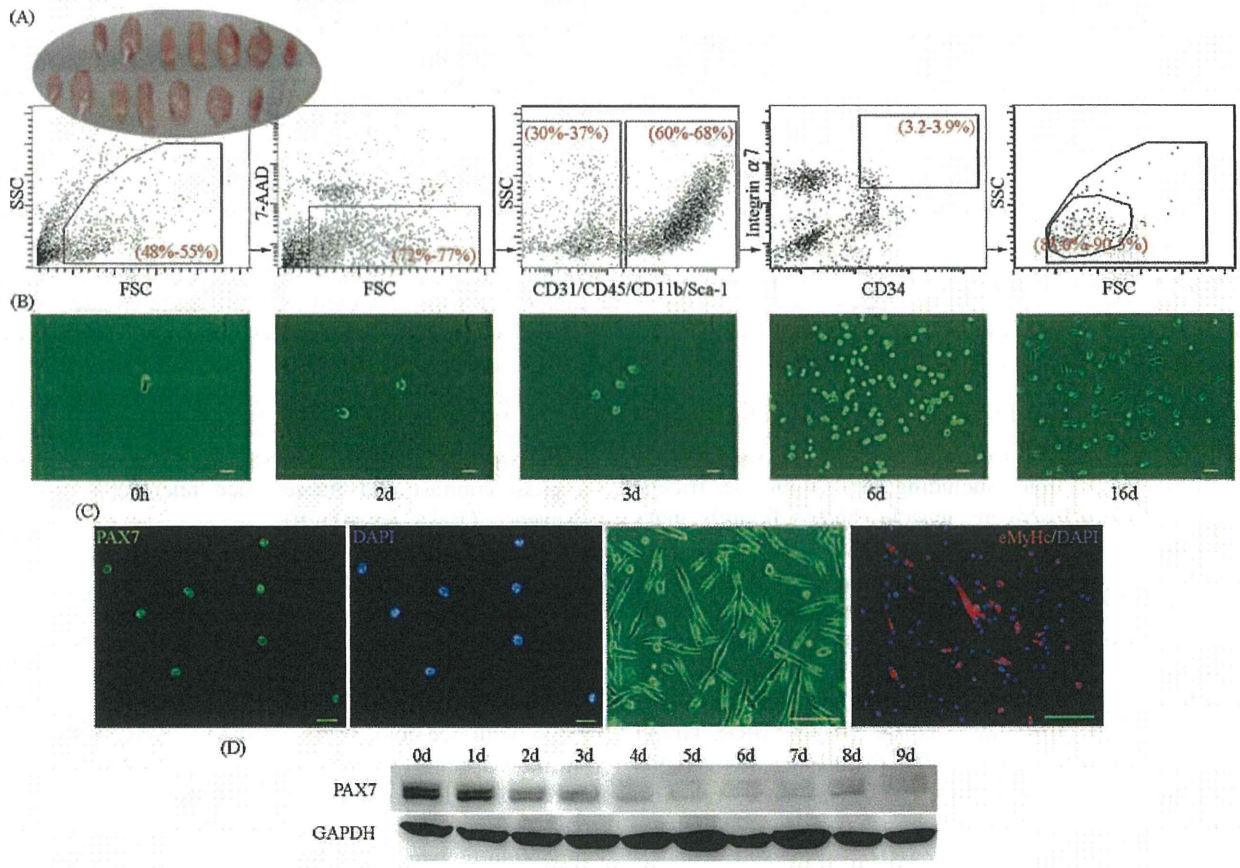

Figure 1. The isolation and characterization of the satellite cells. (**A**) A flow cytometer sorted the satellite cells from the hind-limb muscles after enzymatic dissociation (shown in circle on the left: upper muscles were isolated from a right leg and lower muscles were isolated from a left leg; from left to right: tibialis anterior, triceps surae, quadriceps, divided biceps femoris into two, gluteus maximus, and iliopsoas muscles) by gating for 7-AAD negative, then for CD31, CD45, CD11b, and Sca1 negative, and finally for integrin-α7 and CD34 positive. Numbers in the gates show percentage of the cells in each gate among total cells. (**B**) The light phase-contrast microscopy shows the morphology of the isolated satellite cells cultured in proliferation medium for the indicated time periods. Scale bars: 50 μm (left three panels) and 25 μm (right two panels). (**C**) The sorted cells were immunoreactive with satellite cell marker Pax7 and nucleus marker DAPI after 2 days in the proliferation medium (left two panels: Pax7 in green and DAPI in blue). After 3 days in the differentiation medium, some cells formed tube-like shapes (the third panel from the left) and some cells were immunoreactive with an immature myotube marker eMyHc (right panel: eMyHc in red and DAPI in blue). Scale bars: 20 μm (left two panels) and 50 μm (right two panels). (**D**) Western blot analysis shows the levels of PAX7 protein in the satellite cells after the induction of differentiation for the indicated time periods. The GAPDH protein is a loading control.

iliopsoas muscle) and sorted them according to the cell surface markers (Figure 1A). We characterized satellite cells as 7-AAD (a dead cell marker) negative, CD31 (an endothelial cell marker) negative, CD45 (a pan-hematopoietic cell marker) negative, CD11b (a myeloid cell marker) negative, Sca1 (a mesenchymal cell marker) negative, and integrin-α7 and CD34 positive (Figure 1A). We cultured the sorted cells in growth medium for several days and noted the proliferation of these cells, which suggested that these cells had the potential to re-enter the cell cycle (Figure 1B). After 2 days in the growth medium, the sorted cells were immunoreactive with satellite cell–specific transcriptional factor Pax7 and nucleus marker DAPI (Figure 1C, two panels in the left). To examine the potential of these cells to differentiate into myotubes, we cultured the cells in differentiation medium for 3 days (Figure 1C, two panels in the right). The cells fused and were immunoreactive with an immature myotube marker embryonic myosin heavy chain (eMyHc, Figure 1C, the right panel), suggesting that the cells differentiated into myotubes. The sorted cells were cultured in the differentiation medium, and the expression levels of Pax7 gradually decreased in a time-dependent manner after the induction of differentiation (Figure 1D). These data suggested that the sorted cells had the characteristics of satellite cells and the potential to differentiate into myotubes.

Effects of RJ/pRJ on the Satellite Cells of the Aged Mice In Vitro

To examine the effect of RJ/pRJ on the proliferation rate of the satellite cells of the aged mice in vitro, we isolated satellite cells from aged mice and stimulated them with RJ/pRJ for 24 hours (Figure 2A, left panel), 48 hours (Figure 2A, center panel), or 72 hours (Figure 2A, right

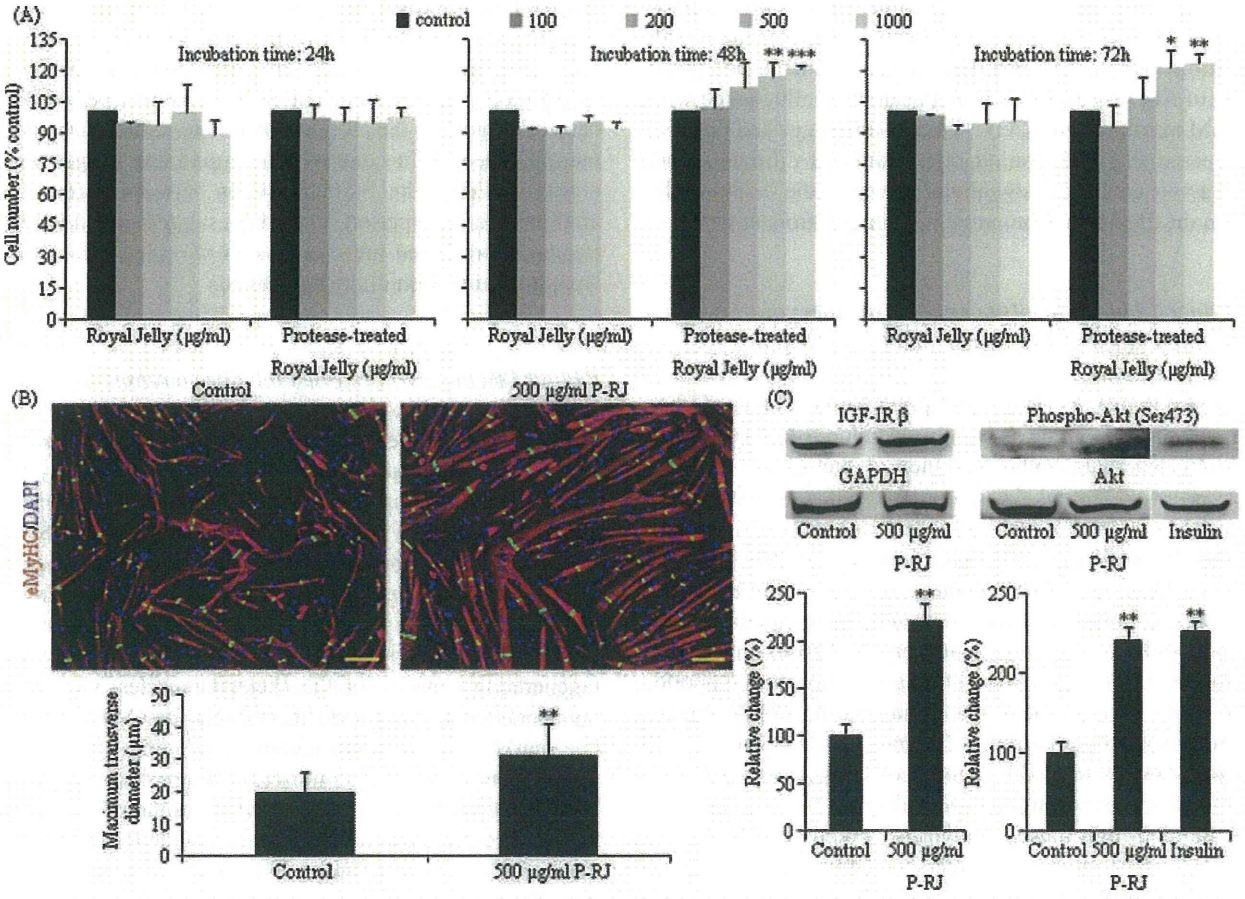

Figure 2. Effects of RJ/pRJ on the satellite cells of aged mice in vitro. (**A**) The satellite cells of the aged mice were treated with the indicated concentrations of RJ or pRJ for 24, 48, or 72 h, and the cell proliferation rate was measured at each time point. (**B**) The satellite cells of aged mice were cultured in differentiation medium with pRJ or without pRJ (control) for 5 days, then immunohistochemically stained for eMyHC in red and for DAPI in blue to evaluate their differentiation into myotubes. The maximum diameter of each myotube was marked with a green line (upper panels). We randomly selected 50 myotubes per field at ×400 magnification, measured the maximum diameter of each myotube for 10 randomly selected fields per sample, measured the diameter, and calculated for each group (lower panel). Scale bars: 100 μm. (**C**) The satellite cells of aged mice were pretreated with pRJ (500 μg/mL) for 48 h, then the Western blot analysis detected IGF-1 receptor (IGF-IR), GAPDH, activated form of Akt (phospho-Akt), and total Akt. Insulin (10 nM) was used as a positive control. The densitometry quantified the band intensities. The graphs show the IGF-IR band intensities normalized by the GAPDH band intensities, and phospho-Akt band intensities normalized by the Akt band intensities. This figure is the representative of three independent experiments. Columns are mean ± *SD*. $^{*}p < .05$, $^{**}p < .01$, and $^{***}p < .0001$, compared with control.

panel) in growth medium. pRJ treatment at high concentrations (500 and 1000 μg/mL) for 48 and 72 hours increased the proliferation rate of the satellite cells compared with controls and RJ treatment (Figure 2A). Next, to examine the effect of RJ/pRJ on the differentiation of the satellite cells of the aged mice in vitro, we cultured the satellite cells in differentiation medium for 5 days and immunohistochemically stained them for eMyHC (Figure 2B). The pRJ-treated group had more eMyHc immunoreactive areas than did the controls (Figure 2B, upper panel). The mean maximum diameter of the myotubes was greater in the pRJ-treated group than in the controls (Figure 2, lower panel). These results suggested that pRJ promoted the differentiation of the satellite cells of the aged mice. We next examined an intracellular signaling pathway of IGF-1 by Western blot analysis. pRJ treatment increased the intensity of the band of IGF-1R compared with controls (Figure 2C). One of the downstream signaling pathways of IGF-1R is Akt, and pRJ treatment increased the intensity of the band of phosphorylated Akt, which is an activated form of Akt, compared with controls (Figure 2C). Similar to pRJ, the increased activation of Akt was also observed in satellite cells treated with 10 nM insulin (Figure 2C). These results suggested that pRJ increased the proliferation rate, promoted differentiation, and activated the Akt-signaling pathway in the satellite cells from the aged mice compared with the controls in vitro.

RJ-/pRJ-Treated Mice Had Greater Numbers of Satellite Cells, Muscle Weight, and Grip Strength Than Did Controls

To examine the effects of RJ/pRJ treatment on aged mice in vivo, we divided 21-month-old mice into five groups and treated them with five kinds of diets for 3 months, respectively: normal diet (controls), diet mixed with 1% weight RJ (1% RJ), diet with 5% weight RJ (5% RJ), diet with 1% weight pRJ (1% pRJ), and diet with 5% pRJ (5% pRJ). Three mice in the controls, one mouse in the 1% RJ group, and one mouse in the 1% pRJ group died of natural causes during the treatment period. These mice were excluded from the analysis. During the intervention period, the body weight increased similarly in RJ/pRJ-treated groups and control groups (Figure 3A) (p value $> .73$; effect size ≤ 0.01). The amount of daily diet intake was not different between the groups (Figure 3B). Comparison of the hind-limb muscle weight per body weight between 2-, 8-, and 24-month-old mice showed progressive loss of muscle weight with aging, suggesting the progression of sarcopenia with aging (Figure 3C). The combined weights of the hind-limb muscles of one leg, named one-legged muscle, per body weight in 5% RJ, 1% pRJ, and 5% pRJ groups were greater than those of controls (Figure 3D). The selected muscles included the TA, triceps surae, quadriceps, biceps femoris, gluteus maximus, and iliopsoas muscles. To examine the effect of PJ/pRJ on the numbers of satellite cells in vivo, we counted the cells. The numbers of satellite cells in the hind-limb muscles in the 5% RJ- and 5% pRJ-treated groups were significantly greater than those of the controls (Figure 3E), whereas the numbers of the satellite cells per muscle weight were not different among the groups (per gram; Figure 3F). These results suggested that PJ/pRJ treatment increased the total numbers of satellite cells.

To examine the effect of pRJ on the muscle strength, we performed the wire hang test and measured the maximum duration that the mice could hang on the inverted wire mesh. Consistent with the effect of RJ/pRJ on the muscle mass, the 5% RJ- and 5% pRJ-treated groups hung for longer duration than did the controls, suggesting that RJ/pRJ improved the grip strength of the skeletal muscles (Figure 3G). To examine the effect of RJ/pRJ on muscle fatigue, we measured how many times the mice could hang from the wire mesh. The 5% RJ- and 5% pRJ-treated groups could hang more times than the controls, suggesting that RJ/pRJ improved the fatigue of the skeletal muscles (Figure 3H). Furthermore, within the controls, comparison of the before and after treatment period showed decreased hanging duration and times after the treatment period than before, suggesting the progression of age-related atrophy in muscle function. In contrast, no significant changes were observed within the RJ/pRJ groups between before and after the treatment period. These data suggested that RJ/pRJ treatment prevented the progression of atrophy in muscle weight and function in the aged mice.

RJ/pRJ Treatment Accelerated the Regeneration of Injured Skeletal Muscles

We next examined the effect of RJ/pRJ treatment on the regenerating capacity of the skeletal muscles in aged mice in vivo by injuring the TA muscles with cardiotoxin injection and observing their regeneration. We isolated the muscles 5 days after the cardiotoxin injection and subjected them to staining. Hematoxylin and eosin staining showed greater amounts of muscle fibers in the RJ/pRJ groups than in the controls (Figure 4A, upper panels). To confirm the regenerating capacity of the skeletal muscles, we immunohistochemically stained the muscles for eMyHc, which is a marker of immature myotubes including regenerating muscles but not of mature muscles (Figure 4A, middle line panels). Quantification of the eMyHc immunoreactive area showed greater immunoreactive areas in the RJ/pRJ groups than in the controls (Figure 4B). These results suggested that RJ/pRJ treatment accelerated the regeneration of the injured skeletal muscles.

RJ/pRJ Treatment Increased Serum IGF-1 Levels

Because RJ has been suggested to have an anti-inflammatory effect, we examined the effect of RJ/pRJ treatment on serum proinflammatory mediator levels in the aged mice.

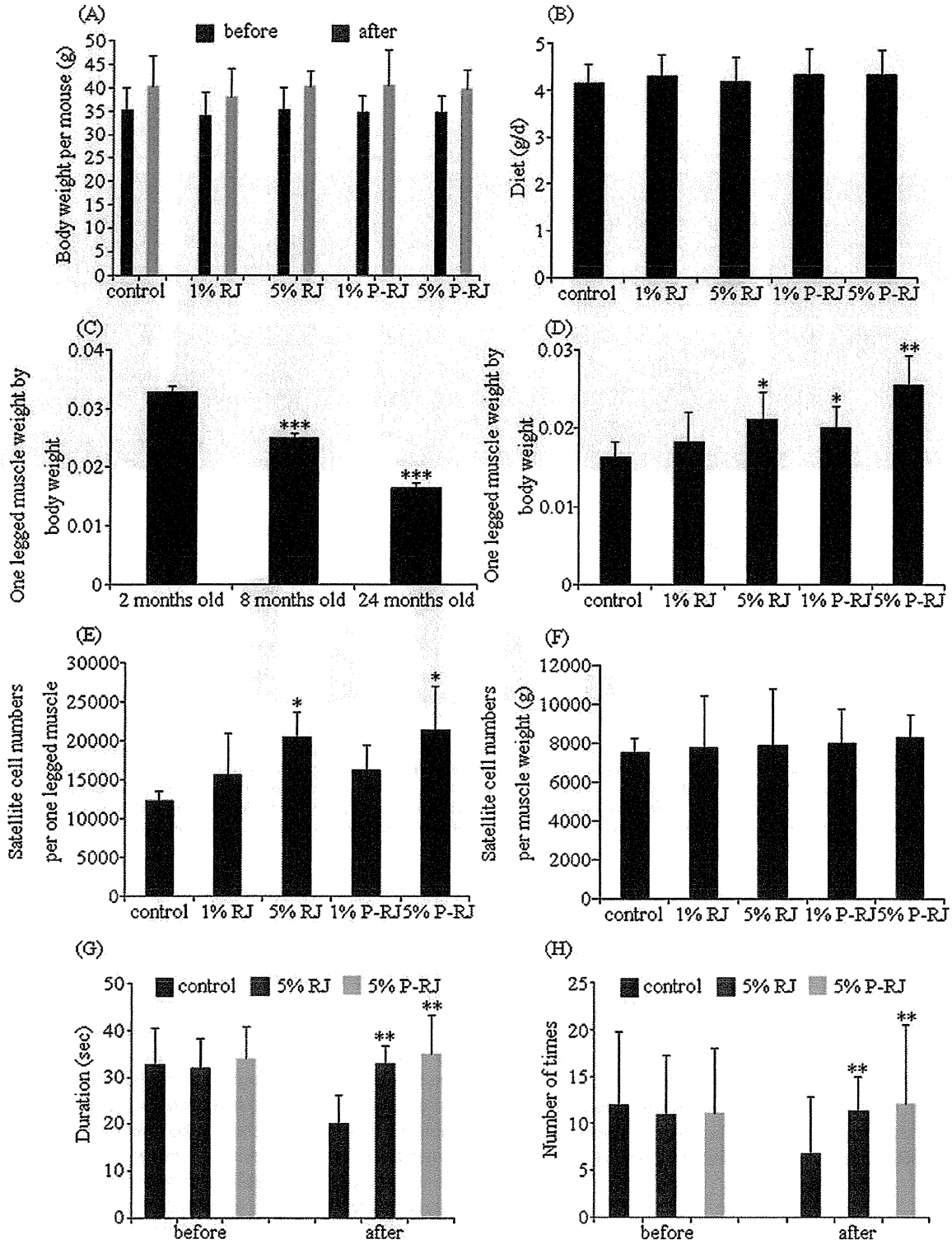

Figure 3. Effects of RJ/pRJ treatment on aged mice in vivo. Twenty-one-month-old mice were treated with a diet mixed with 1% weight RJ (1% RJ), diet with 5% weight RJ (5% RJ), diet with 1% weight pRJ (1% pRJ), or diet with 5% pRJ (5% pRJ) for following 3 months. (**A**) Control, RJ, or pRJ treatment did not show changed body weight. (**B**) RJ or pRJ did not change the amount of the daily diet intake. (**C**) The progressive loss of muscle weight with aging. (**D**) RJ- and pRJ-treated groups had greater hind-limb muscle weights per body weight than did controls. (**E**) RJ- and pRJ-treated groups had greater numbers of satellite cells in the hind-limb muscles than did controls. (**F**) RJ or pRJ treatment did not change the numbers of satellite cells per muscle weight (g). (**G**) Five% RJ- and pRJ-treated mice hung for longer durations than did controls. (**H**) Five% RJ- and pRJ-treated mice hung more times than did controls. Columns are mean ± *SD*, $n \geq 5$ in each group. *$p < .05$, **$p < .01$, and ***$p \leq .0001$ compared with control.

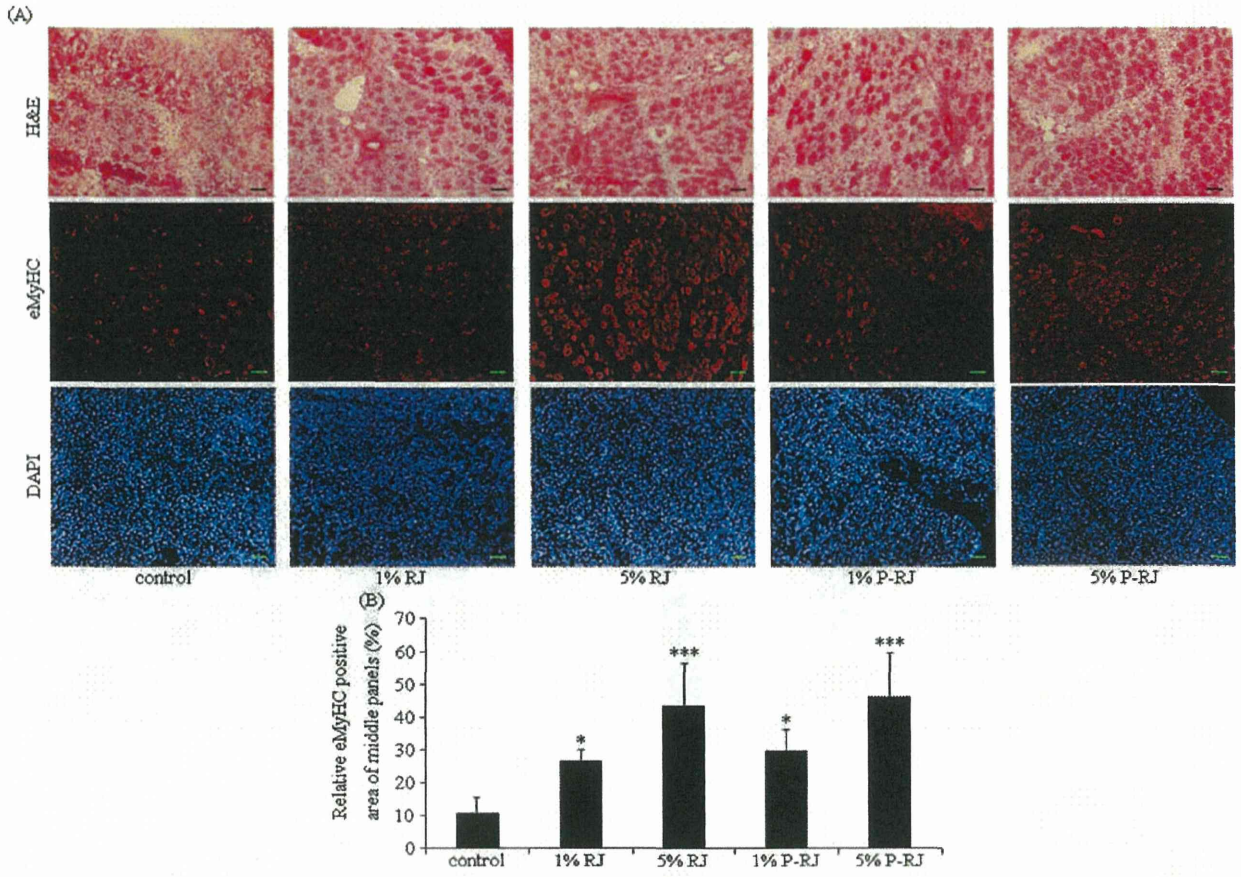

Figure 4. RJ/pRJ treatment accelerated the regeneration of the injured skeletal muscles in aged mice. After 3 months of RJ/pRJ treatment, we injected cardiotoxin into the tibialis anterior muscles of the aged mice to injure the muscles and isolated them 5 days later. (**A**) Hematoxylin and eosin staining (top panels) and immunohistochemical staining for eMyHC (middle panels) or DAPI (bottom panels) of the injured tibialis anterior muscles. Upper lines, scale bar, 50 μm; middle and lower lines, scale bar, 100 μm. (**B**) The graph shows the data calculated from quantification of the percentage of eMyHc-immunoreactive area per field for each group (10 randomly selected fields at ×200 magnification per sample were quantified). Columns are mean ± *SD*, $n \geq 3$ in each group. $^{*}p < .05$, and $^{***}p < .0001$ compared with controls.

We chose IL-1α, IL-1β, IL-6, and tumor necrosis factor-α as proinflammatory mediators, as previously shown (31,32), and measured their levels in serum. The levels of these mediators were not significantly different between RJ-/pRJ-treated groups and controls, but the serum IL-1α concentration tended to be lower in the RJ/pRJ groups than in the controls (Figure 5A). Because IGF-1 plays a central role in stimulating satellite cells, we measured the serum levels of IGF-1. The serum levels of IGF-1 were greater in the 5% RJ- and pRJ-treated groups than in the controls (Figure 5B).

Discussion

In this study, using aged mice, we showed that RJ/pRJ treatment increased the number of satellite cells, the skeletal muscle weight, grip strength, regenerating capacity of injured skeletal muscles, and the serum IGF-1 levels compared with controls in vivo. In vitro, compared with controls, pRJ treatment increased the cell proliferation rate, promoted differentiation, and activated the Akt-signaling pathway in the satellite cells of the aged mice.

RJ/pRJ treatment increased the number of satellite cells of the aged mice, promoted their differentiation compared with controls, which could be the mechanisms by which the skeletal muscle weight and grip strength were increased, and accelerated the regeneration of injured skeletal muscles in aged mice compared with controls. Because these effects antagonized the loss of muscle mass and strength, the results suggested that RJ/pRJ treatment might improve sarcopenia in aged mice. The RJ-/pRJ-treated groups hung for longer durations than did the controls, but when we compared between before and after the treatment period within the same groups, the hanging duration did not change in the RJ-/pRJ-treated groups, whereas the hanging duration decreased after the same period in controls, suggesting that RJ/pRJ treatment might not improve but rather attenuated the progression of the decrease in grip strength. Therefore, the effects of RJ/pRJ on skeletal muscles might be

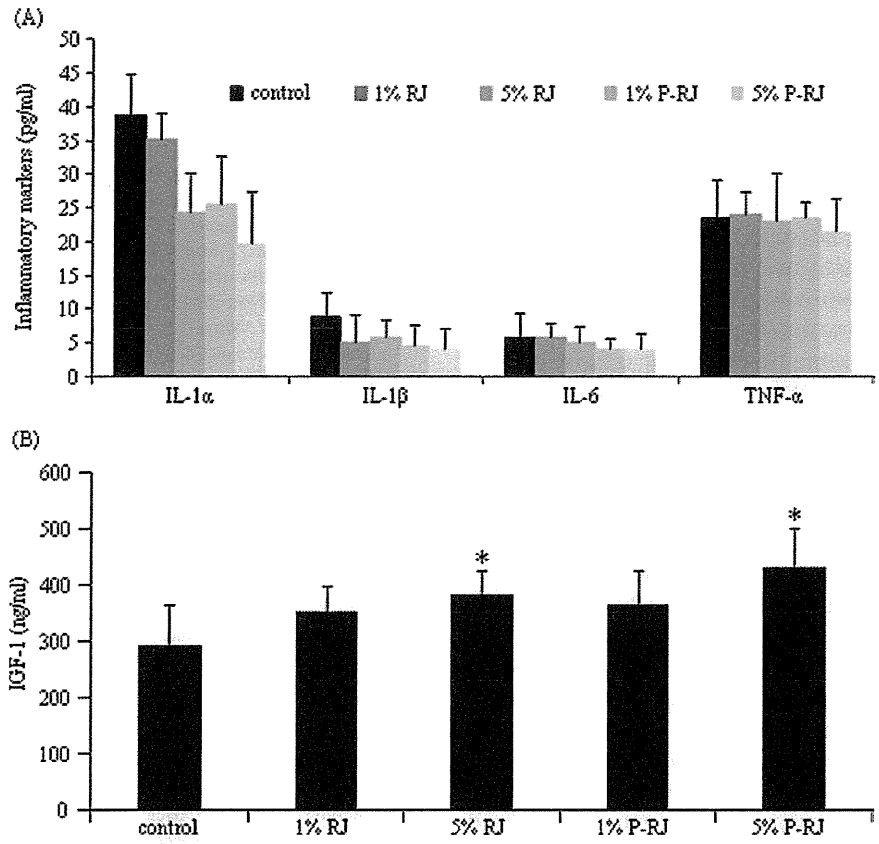

Figure 5. RJ/pRJ treatment increased the serum IGF-1 levels but did not affect the serum proinflammatory mediator levels. ELISA determined serum levels of proinflammatory mediators and IGF-1 in aged mice treated with RJ/pRJ for 3 months. (**A**) RJ/pRJ treatment did not change the serum levels of the proinflammatory mediators. (**B**) Five% RJ and 5% pRJ treatment significantly increased the serum IGF-1 levels. Columns are mean ± *SD*, $n = 5$ in each group. *$p < .05$ compared with controls.

attenuating the atrophy rather than improving the muscle mass and strength in aged mice.

pRJ increased the number of satellite cells of the aged mice in vivo and in vitro, whereas RJ increased the number of the satellite cells in vivo but not in vitro. The presence of protease treatment in pRJ and its absence in RJ might explain this discrepancy. Protease is present in vivo, which indicates that all the RJ is treated with protease after their intake in vivo, whereas protease is not present in vitro.

Because IGF-1 has favorable effects on satellite cells, the skeletal muscles, and sarcopenia, the increased serum levels of IGF-1 after RJ/pRJ treatment might be one of the mechanisms of the effects of RJ/pRJ treatment. However, the increases in the levels of IGF-1 after RJ/pRJ treatment were moderate. Therefore, RJ/pRJ treatment may have other mechanisms besides increasing IGF-1. Previous studies indicated that nutrition plays a central role in the regulation of the IGF-1 levels (33). The serum IGF-1 levels decline in an age-dependent manner and are a reliable index of protein-energy malnutrition in elderly patients (34–36). Increased serum levels of IGF-1 after RJ/pRJ treatment may suggest that RJ/pRJ treatment improved the malnutrition in the aged animals. Many nutritional components in RJ/pRJ such as vitamins, minerals (Table 1), and amino acids might have contributed to preventing sarcopenia. Because this is a single study, we could not evaluate the contribution of each component to the prevention of sarcopenia. However, the results suggested that whole RJ/pRJ improved sarcopenia in aged mice.

Akt-signaling pathway plays a central role in muscle protein synthesis and in inhibiting muscle proteolysis. Akt activation prevents muscle atrophy including sarcopenia (37). Moreover, the activation of Akt in myoblasts increased their cell proliferation rate and rescued them from cell death (22). In vitro, pRJ activated the Akt-signaling pathway in satellite cells of the aged mice. Because pRJ contains a wide variety of components (9), it is not clear which component(s) activated Akt. However, the activation of Akt, possibly by IGF-1, suggests that one of the mechanisms of the effects of RJ/pRJ was via Akt. Furthermore, because RJ and pRJ are natural products, some natural factors such as seasonal or environmental factors may affect the percentage or quality of ingredients in RJ/pRJ. Further studies are required to identify the mechanisms of action of RJ/pRJ.

Some studies reported that IGF-1 deficiency extended life spans in mammals (38,39). Because we did not assess life

spans in this study, the effect of increased levels of IGF-1 by RJ/pRJ treatment on life span was not clear. However, previous studies reported that RJ/pRJ extended the life span in mice and *Caenorhabditis elegans* (10,11). Further studies are required to evaluate the effects and mechanisms of RJ/pRJ on life span.

Dietary supplementation with 1%–5% RJ/pRJ would be too great in an amount and would not be feasible for humans. Generally, dietary supplementation intake in animals cannot be directly converted into human dietary intake. Thus, we did a pilot study to examine the effect of RJ on muscle strength and physical performance in free-living elderly patients (Identifier: UMIN000004057, Trial Registration: http://www.umin.ac.jp/ctr/index.htm). We found that the intake of RJ (low dose: 1.2 g/day; high dose: 4.8 g/day) for 3 months improved muscle strength and physical performance in the elderly patients. Based on this pilot study, we are performing a randomized, double-blinded, placebo-controlled trial to confirm the effects of RJ on muscle strength and physical performance of the elderly patients (Identifier: UMIN000009648, Trial Registration: http://www.umin.ac.jp/ctr/index.htm).

In conclusion, in vivo, RJ/pRJ treatment increased the muscle weight, grip strength, regenerating capacity of injured muscles, and serum IGF-1 levels compared with controls in aged mice. In vitro, pRJ increased the cell proliferation rate, promoted the cell differentiation, and activated Akt-signaling pathway compared with controls in isolated satellite cells from aged mice. These findings suggest that RJ/pRJ treatment may have a beneficial effect on the prevention of age-related sarcopenia through increasing the systemic IGF-1 levels and activating Akt-signaling pathways in satellite cells.

FUNDING

This research was supported by Yamada Research Grant.

CONFLICT OF INTERESTS

All the authors have no conflicts of interest to disclose.

REFERENCES

1. Nations United. *Department of Economic and Social Affairs Population Division: World Population Ageing 2009*. New York: United Nations; 2009:11.
2. Altun M, Grönholdt-Klein M, Wang L, Ulfhake B. Cellular degradation machineries in age-related loss of muscle mass (Sarcopenia). In: Nagata T, ed. *Senescence*. San Francisco, CA: Academia.edu; 2012:269–286.
3. Hawke TJ, Garry DJ. Myogenic satellite cells: physiology to molecular biology. *J Appl Physiol*. 2001;91:534–551.
4. Clemmons DR. Role of IGF-I in skeletal muscle mass maintenance. *Trends Endocrinol Metab*. 2009;20:349–356.
5. Welle S. Cellular and molecular basis of age-related sarcopenia. *Can J Appl Physiol*. 2002;27:19–41.
6. Sacco A, Doyonnas R, Kraft P, Vitorovic S, Blau HM. Self-renewal and expansion of single transplanted muscle stem cells. *Nature*. 2008;456:502–506.
7. Giovannini S, Marzetti E, Borst SE, Leeuwenburgh C. Modulation of GH/IGF-1 axis: potential strategies to counteract sarcopenia in older adults. *Mech Ageing Dev*. 2008;129:593–601.
8. Viuda-Martos M, Ruiz-Navajas Y, Fernández-López J, Pérez-Alvarez JA. Functional properties of honey, propolis, and royal jelly. *J Food Sci*. 2008;73:R117–R124.
9. Sabatini AG, Marcazzan GL, Caboni MF, Bogdanov S, Almeida-Muradian LBd. Quality and standardisation of Royal Jelly. *J ApiProduct ApiMedical Sci*. 2009;1:1–6.
10. Inoue S, Koya-Miyata S, Ushio S, Iwaki K, Ikeda M, Kurimoto M. Royal Jelly prolongs the life span of C3H/HeJ mice: correlation with reduced DNA damage. *Exp Gerontol*. 2003;38:965–969.
11. Honda Y, Fujita Y, Maruyama H, et al. Lifespan-extending effects of royal jelly and its related substances on the nematode Caenorhabditis elegans. *PLoS One*. 2011;6:e23527.
12. Kamakura M, Mitani N, Fukuda T, Fukushima M. Antifatigue effect of fresh royal jelly in mice. *J Nutr Sci Vitaminol (Tokyo)*. 2001;47:394–401.
13. Matsui T, Yukiyoshi A, Doi S, Sugimoto H, Yamada H, Matsumoto K. Gastrointestinal enzyme production of bioactive peptides from royal jelly protein and their antihypertensive ability in SHR. *J Nutr Biochem*. 2002;13:80–86.
14. Vittek J. Effect of royal jelly on serum lipids in experimental animals and humans with atherosclerosis. *Experientia*. 1995;51:927–935.
15. Liu JR, Yang YC, Shi LS, Peng CC. Antioxidant properties of royal jelly associated with larval age and time of harvest. *J Agric Food Chem*. 2008;56:11447–11452.
16. Kohno K, Okamoto I, Sano O, et al. Royal jelly inhibits the production of proinflammatory cytokines by activated macrophages. *Biosci Biotechnol Biochem*. 2004;68:138–145.
17. Macaluso A, De Vito G. Muscle strength, power and adaptations to resistance training in older people. *Eur J Appl Physiol*. 2004;91:450–472.
18. Strasser EM, Wessner B, Roth E. Cellular regulation of anabolism and catabolism in skeletal muscle during immobilisation, aging and critical illness. *Wien Klin Wochenschr*. 2007;119:337–348.
19. Schaap LA, Pluijm SM, Deeg DJ, Visser M. Inflammatory markers and loss of muscle mass (sarcopenia) and strength. *Am J Med*. 2006;119:526.e9–526.17.
20. Meng SJ, Yu LJ. Oxidative stress, molecular inflammation and sarcopenia. *Int J Mol Sci*. 2010;11:1509–1526.
21. Sriram S, Subramanian S, Sathiakumar D, et al. Modulation of reactive oxygen species in skeletal muscle by myostatin is mediated through NF-κB. *Aging Cell*. 2011;10:931–948.
22. Okazaki T, Ebihara S, Asada M, et al. Macrophage colony-stimulating factor improves cardiac function after ischemic injury by inducing vascular endothelial growth factor production and survival of cardiomyocytes. *Am J Pathol*. 2007;171:1093–1103.
23. Yahiaoui L, Gvozdic D, Danialou G, Mack M, Petrof BJ. CC family chemokines directly regulate myoblast responses to skeletal muscle injury. *J Physiol*. 2008;586:3991–4004.
24. Okazaki T, Ebihara S, Asada M, Yamanda S, Niu K, Arai H. Erythropoietin promotes the growth of tumors lacking its receptor and decreases survival of tumor-bearing mice by enhancing angiogenesis. *Neoplasia*. 2008;10:932–939.
25. Nakajima R, Takao K, Huang SM, et al. Comprehensive behavioral phenotyping of calpastatin-knockout mice. *Mol Brain*. 2008;7:1–15.
26. Uezumi A, Fukada S, Yamamoto N, Takeda S, Tsuchida K. Mesenchymal progenitors distinct from satellite cells contribute to ectopic fat cell formation in skeletal muscle. *Nat Cell Biol*. 2010;12:143–152.
27. Niu K, Asada M, Okazaki T, et al. Adiponectin pathway attenuates malignant mesothelioma cell growth. *Am J Respir Cell Mol Biol*. 2012;46:515–523.
28. Fukada S, Yamaguchi M, Kokubo H, et al. Hesr1 and Hesr3 are essential to generate undifferentiated quiescent satellite cells and to maintain satellite cell numbers. *Development*. 2011;138:4609–4619.
29. Asada M, Ebihara S, Yamanda S, et al. Depletion of serotonin and selective inhibition of 2B receptor suppressed tumor angiogenesis by

inhibiting endothelial nitric oxide synthase and extracellular signal-regulated kinase ½ phosphorylation. *Neoplasia*. 2009;11:408–417.
30. Yamanda S, Ebihara S, Asada M, et al. Role of ephrinB2 in non-productive angiogenesis induced by Delta-like 4 blockade. *Blood*. 2009;113:3631–3639.
31. Okazaki T, Sakon S, Sasazuki T, et al. Phosphorylation of serine 276 is essential for p65 NF-kappaB subunit-dependent cellular responses. *Biochem Biophys Res Commun*. 2003;300:807–812.
32. Okazaki T, Ni A, Baluk P, et al. Capillary defects and exaggerated inflammatory response in the airways of EphA2-deficient mice. *Am J Pathol*. 2009;174:2388–2399.
33. Chevenne D, Porquet D. Growth hormone (GH) and insulin-like growth factor 1 (IGF-1) in nutritional status. *Ann Biol Clin (Paris)*. 1995;53:527–538.
34. Campillo B, Paillaud E, Bories PN, Noel M, Porquet D, Le Parco JC. Serum levels of insulin-like growth factor-1 in the three months following surgery for a hip fracture in elderly: relationship with nutritional status and inflammatory reaction. *Clin Nutr*. 2000;19:349–354.
35. Ponzer S, Tidermark J, Brismar K, Söderqvist A, Cederholm T. Nutritional status, insulin-like growth factor-1 and quality of life in elderly women with hip fractures. *Clin Nutr*. 1999;18:241–246.
36. McWhirter JP, Ryan MF, Pennington CR. An evaluation of insulin-like growth factor-1 as an indicator of nutritional status. *Clin Nutr*. 1995;14:74–80.
37. Kandarian SC, Jackman RW. Intracellular signaling during skeletal muscle atrophy. *Muscle Nerve*. 2006;33:155–165.
38. Carter CS, Ramsey MM, Ingram RL, et al. Models of growth hormone and IGF-1 deficiency: applications to studies of aging processes and lifespan determination. *J Gerontol A Biol Sci Med Sci*. 2002;57:B177–B188.
39. Chiba T, Yamaza H, Shimokawa I. Role of insulin and growth hormone/insulin-like growth factor-I signaling in lifespan extension: rodent longevity models for studying aging and calorie restriction. *Curr Genomics*. 2007;8:423–428.

Cardiac Positron-Emission Tomography Images With an Amyloid-Specific Tracer in Familial Transthyretin-Related Systemic Amyloidosis

Katsutoshi Furukawa, MD, PhD; Shu-ichi Ikeda, MD, PhD; Nobuyuki Okamura, MD, PhD; Manabu Tashiro, MD, PhD; Naoki Tomita, MD, PhD; Shozo Furumoto, PhD; Ren Iwata, PhD; Kazuhiko Yanai, MD, PhD; Yukitsuka Kudo, PhD; Hiroyuki Arai, MD, PhD

We report the case of a 32-year-old man who had suffered from orthostatic syncope and body weight loss since he was 27 years old. As years passed by, he also showed muscle weakness and abnormal sensations in both legs, hyporeflexia in 4 limbs, and autonomic failure (impotence, urinary and fecal incontinence, and edema in lower limbs) suggesting the presence of peripheral somatic and autonomic polyneuropathy. His mother, mother's father, and mother's paternal aunt also had similar symptoms. Both the sensory nerve action potential and the sensory nerve conduction velocity of his right sural nerve were low (1.26 μV and 47.2 m/s, respectively), and the motor nerve conduction velocity of his right tibial nerve was 41.1 m/s (normal >45 m/s). A DNA test on the man disclosed a missense mutation in the transthyretin gene (Ser50Arg), which is relatively rare in familial transthyretin-related systemic amyloidosis.[1,2] Transthyretin-immunoreactive amyloid deposition was demonstrated in the biopsied gastroduodenal mucosa (Figure 1). Echocardiography showed a markedly thickened ventricular wall (thickness of interventricular septum 22.3 mm [normal <12 mm]) with normal wall motion (fractional shortening 37.6% [normal 28–42%]), indicating that he also had cardiac

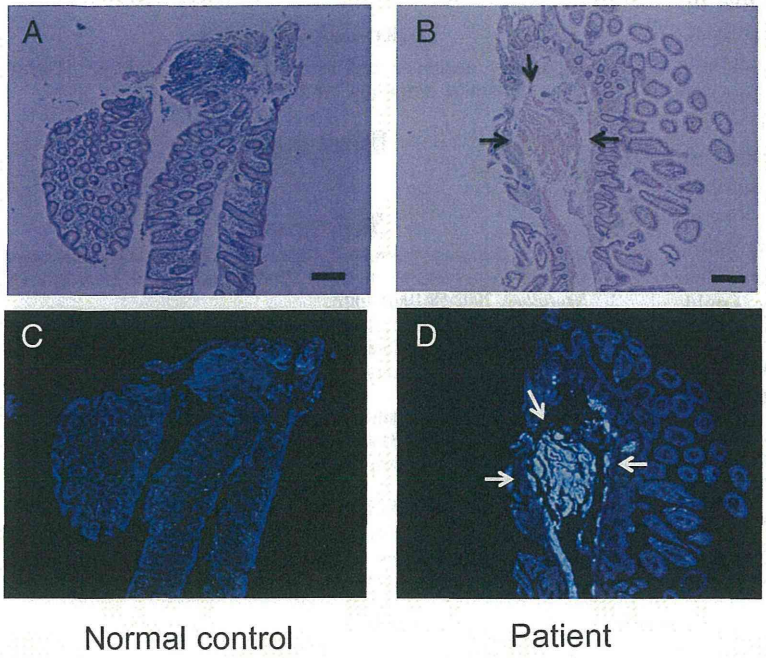

Figure 1. Detection of amyloid deposition in the intestines. Congo red (**A** and **B**) and BF-227 (**C** and **D**) clearly detect transthyretin in the submucosal space of the small intestine of the patient. Scale bars, 100 μm.

From the Department of Geriatrics and Gerontology, Division of Brain Sciences, Institute of Development, Aging and Cancer, Tohoku University (K.F., N.T., H.A.); Department of Medicine (Neurology & Rheumatology), Shinshu University School of Medicine (S.I.); Department of Pharmacology, Tohoku University Graduate School of Medicine (N.O., S.F., K.Y.); Division of Cyclotron Nuclear Medicine, Cyclotron and Radioisotope Center, Tohoku University (M.T.); Division of Radiopharmaceutical Chemistry, Cyclotron and Radioisotope Center, Tohoku University (R.I.); Department of NeuroImaging Research, Innovation New Biomedical Engineering Center, Tohoku University (Y.K.), Sendai, Japan.

Correspondence to Katsutoshi Furukawa, MD, PhD, Department of Geriatrics and Gerontology, Institute of Development, Aging and Cancer, Tohoku University, 4-1 Seiryo-machi Aobaku, Sendai 980-8575 Japan. E-mail kfurukawa-ns@umin.ac.jp

(*Circulation*. 2012;125:556-557.)

Circulation is available at http://circ.ahajournals.org

DOI: 10.1161/CIRCULATIONAHA.111.045237

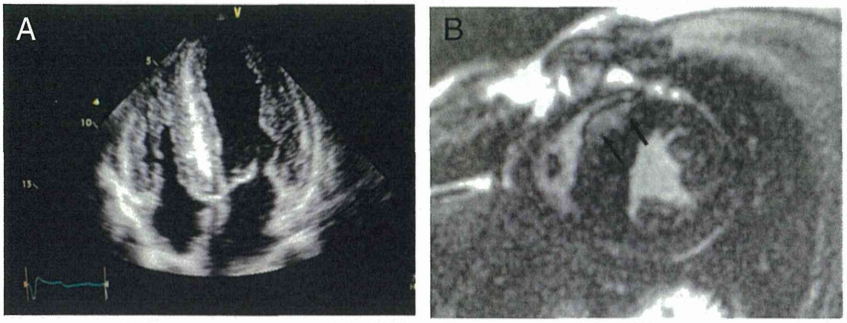

Figure 2. A, Echocardiographic finding. Four chamber views show symmetrical thickening of ventricular walls and septum with hyperrefractile myocardial echo (the so-called granular sparkling appearance). **B**, Contrast magnetic resonance imaging with gadolinium. Focal late gadolinium enhancement is visible (arrows).

amyloidosis (Figure 2A). Contrast magnetic resonance imaging[3] revealed focal late gadolinium enhancement in the thickened ventricular wall (Figure 2B). The patient had been treated with orthotopic live-donor liver transplantation when he was 31 years old to alleviate and prevent exacerbation of his neuronal and cardiac symptoms. His condition, including the neurological disability, gradually improved, and he started to work again 10 months after liver transplantation.

In order to visualize amyloid deposition in the myocardium, the patient underwent a cardiac positron-emission tomography study with [^{11}C]-BF-227 that sensitively and specifically binds to aggregated amyloid fibrils.[4] The positron-emission tomography images revealed significantly robust retention of [^{11}C]-BF-227 in the patient's heart compared with that of the normal control (Figure 3). Biopsy specimens from the patient's duodenum also showed higher signals of BF-227 compared with that of the normal control (Figure 1, C and D). The present result provides evidence that our amyloid-specific positron-emission tomography tracer, [^{11}C]-BF-227, can successfully detect amyloid deposition in the heart. Several molecules, such as ^{99m}Tc-aprotinin and ^{99m}Tc-labeled phosphate derivatives, have been investigated to visualize cardiac amyloidosis.[2] None of the previous tracers, however, could specifically bind to aggregated amyloid, which forms a β-pleated sheet structure. In any of the amyloidgenic disorders, such as transthyretin-related systemic amyloidosis and Alzheimer's disease, it is surmised that the monomer of the amyloid protein itself is not very toxic, whereas misfolded oligomers could cause damage to human organs.[1–4] It is therefore truly important to detect the accumulation of real amyloid fibrils for the early and accurate diagnosis of amyloidosis. To our knowledge, this is the first report showing the usefulness of a β-pleated sheet structure-specific positron-emission tomography in investing visceral organ amyloidosis.

Sources of Funding

This study was supported by the Program for the Promotion of Fundamental Studies in Health Science by the National Institute of Biomedical Innovation; the Special Coordination Funds for Promoting Science and Technology; the Industrial Technology Research Grant Program from the New Energy and Industrial Technology Development Organization of Japan; Health and Labor Sciences Research Grants for Translational Research from the Ministry of Health; and the Ministry of Education, Culture, Sports and Technology of Japan.

Acknowledgments

We appreciate technical assistance of Shoichi Watanuki, Yoichi Ishikawa, Motohisa Kato, and Emiko Fukuda.

Disclosures

None.

References

1. Ikeda S, Nakazato M, Ando Y, Sobue G. Familial transthyretin-type amyloid polyneuropathy in Japan: Clinical and genetic heterogeneity. *Neurology*. 2002;58:1001–1007.
2. Rapezzi C, Quarta CC, Riva L, Longhi S, Gallelli I, Lorenzini M, Ciliberti P, Biagini E, Salvi F, Branzi A. Transthyretin-related amyloidoses and the heart: a clinical overview. *Nat Rev Cardiol*. 2010;7:398–408.
3. Vogelsberg H, Mahrholdt H, Deluigi CC, Yilmaz A, Kispert Eva M, Greulich S, Klingel K, Kandolf R, Sechtem U. Cardiovascular magnetic resonance in clinically suspected cardiac amyloidosis. *J Am Coll Cardiol*. 2008;s51:1022–1030.
4. Furukawa K, Okamura N, Tashiro M, Waragai M, Furumoto S, Iwata R, Yanai K, Kudo Y, Arai H. Amyloid PET in mild cognitive impairment and Alzheimer's disease with BF-227: Comparison to FDG-PET. *J Neurol*. 2010;257:721–727.

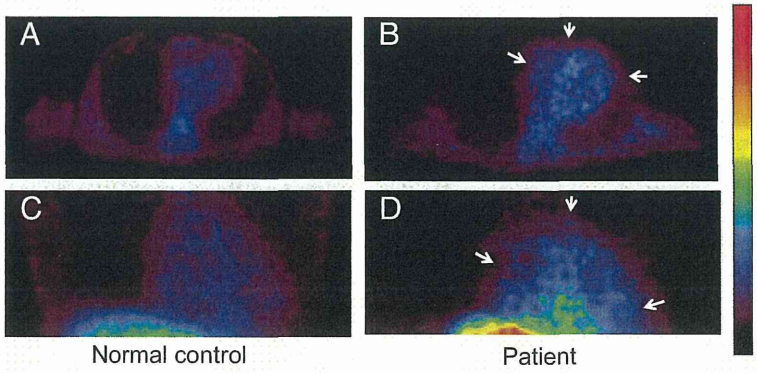

Figure 3. [^{11}C]-BF-227 positron emission tomgraphy succeeds in visualization of amyloid deposition in the heart. Axial and coronal images are **A** and **B** and **C** and **D**, respectively. Arrows indicate high signals of [^{11}C]-BF-227 in the heart of the patient (**B** and **D**).